Unique Role of Dystroglycan in Peripheral Nerve Myelination, Nodal Structure, and Sodium Channel Stabilization

Fumiaki Saito,[1,9] Steven A. Moore,[2,9] Rita Barresi,[1]
Michael D. Henry,[1] Albee Messing,[5]
Susan E. Ross-Barta,[2] Ronald D. Cohn,[1]
Roger A. Williamson,[3] Kathleen A. Sluka,[4]
Diane L. Sherman,[6] Peter J. Brophy,[6]
James D. Schmelzer,[7] Phillip A. Low,[7]
Lawrence Wrabetz,[8] M. Laura Feltri,[8]
and Kevin P. Campbell[1,*]
[1]Howard Hughes Medical Institute
Department of Physiology and Biophysics
Department of Neurology
[2]Department of Pathology
[3]Department of Obstetrics and Gynecology
[4]Physical Therapy and Rehabilitation Science
    Graduate Program
University of Iowa Roy J. and Lucille A. Carver
    College of Medicine
Iowa City, Iowa 52242
[5]Department of Biological Science
School of Veterinary Medicine
Waisman Center
University of Wisconsin
Madison, Wisconsin 53705
[6]Centre for Neuroscience Research
Department of Preclinical Veterinary Sciences
University of Edinburgh
EH9 1QH Edinburgh
United Kingdom
[7]Department of Neurology
Mayo Clinic
Rochester, Minnesota 55905
[8]San Raffaele Scientific Institute
DIBIT
20132 Milano
Italy

Summary

Dystroglycan is a central component of the dystrophin-glycoprotein complex implicated in the pathogenesis of several neuromuscular diseases. Although dystroglycan is expressed by Schwann cells, its normal peripheral nerve functions are unknown. Here we show that selective deletion of Schwann cell dystroglycan results in slowed nerve conduction and nodal changes including reduced sodium channel density and disorganized microvilli. Additional features of mutant mice include deficits in rotorod performance, aberrant pain responses, and abnormal myelin sheath folding. These data indicate that dystroglycan is crucial for both myelination and nodal architecture. Dystroglycan may be required for the normal maintenance of voltage-gated sodium channels at nodes of Ranvier, possibly by mediating trans interactions between Schwann cell microvilli and the nodal axolemma.

*Correspondence: kevin-campbell@uiowa.edu
[9]These authors contributed equally to this work.

Introduction

Dystroglycan (DG) is encoded by a single gene and cleaved into two proteins, α- and β-DG, by posttranslational processing (Ibraghimov-Beskrovnaya et al., 1992). In skeletal muscle, DG is a component of a well-characterized dystrophin-glycoprotein complex. α-DG is an extracellular peripheral membrane protein that strongly binds to laminin in the extracellular matrix (ECM) (Ervasti and Campbell, 1993). The transmembrane protein β-DG anchors α-DG, and the cytoplasmic domain of β-DG interacts with dystrophin, which in turn binds to F-actin (Jung et al., 1995). Thus, DG stabilizes the plasma membrane by acting as an axis through which the ECM is tightly linked to cytoskeleton. Deficiency of any of several DGC components or laminin 2 leads to muscular dystrophy (Cohn and Campbell, 2000; Cohn et al., 2002).
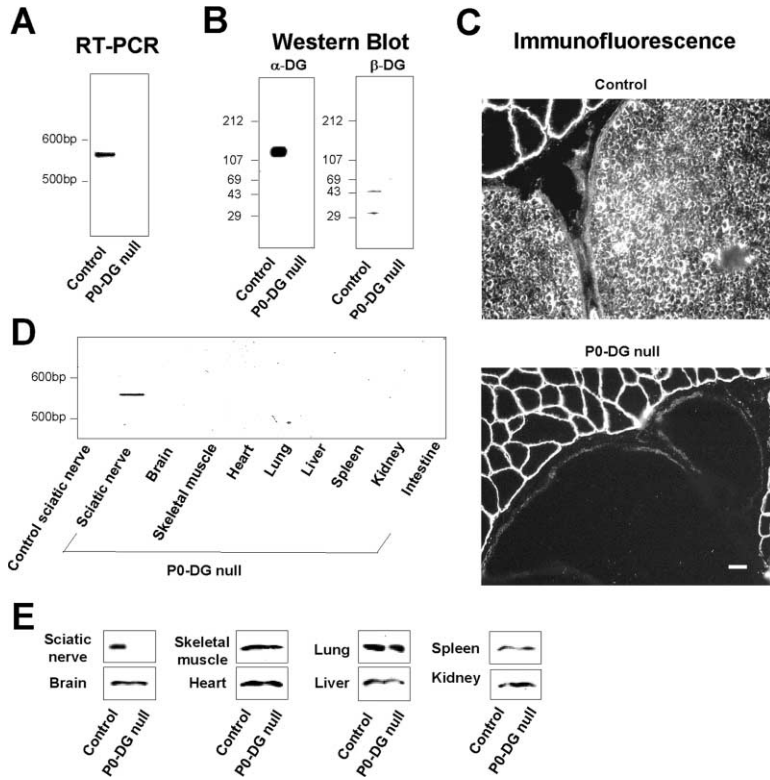
Dystroglycan is widely expressed also by nonmuscle tissues including peripheral nerve (Matsumura et al., 1993). Although DG plays a role in the pathogenesis of *Mycobacterium leprae* (*M. leprae*) neuropathy (Rambukkana et al., 1998), its normal functions in peripheral nerve are unknown. Dystroglycan is expressed by Schwann cells where it localizes to the outer membrane apposing the basal lamina (Yamada et al., 1994; Saito et al., 1999; Masaki et al., 2000). There, DG interacts with laminin 2 and agrin (Yamada et al., 1996) and forms a DGC-like complex with Dp116 (Byers et al., 1993; Saito et al., 1999), a Schwann cell-specific alternatively spliced form of dystrophin, as well as with utrophin and sarcoglycans (Imamura et al., 2000). In addition, the dystrophin related protein 2 (DRP2)-L-periaxin complex binds to DG (Sherman et al., 2001). Importantly, mutations of L-periaxin cause dysmyelinating peripheral neuropathy in humans and mice (Gillespie et al., 2000; Boerkoel et al., 2001; Guilbot et al., 2001). Many studies in vitro have indicated that the basal lamina, especially laminin 2, is important for Schwann cells to ensheath and myelinate axons (Bunge et al., 1993). Furthermore, congenital muscular dystrophy patients and dy/dy mice deficient in laminin 2 develop not only muscular dystrophy, but also dysmyelinating peripheral neuropathy (Matsumura et al., 1997).

These observations prompted us to hypothesize that laminin receptors on the Schwann cell surface play a crucial role in myelination by binding with and conveying signals from laminin 2. Dystroglycan is an excellent candidate for a laminin 2 receptor involved in myelination, because it is coexpressed with laminin 2 during peripheral nerve myelination and regeneration after nerve crush injury (Masaki et al., 2000, 2002). Furthermore, *M. leprae* or *M. leprae* components that bind DGC, such as phenolic glycolipid-1, cause demyelination in vitro and in vivo (Rambukkana et al., 2002).

The constitutive DG knockout is embryonic lethal (Williamson et al., 1997), so to elucidate the role of DG in peripheral nerve, we generated mice in which DG is disrupted selectively in Schwann cells using the P0 protein promoter and Cre-loxP technology. We show that the loss of DG causes severe neurological dysfunction and a broad spectrum of morphological abnormalities

A RT-PCR

600bp –
500bp –

Control
P0-DG null

B Western Blot

α-DG

212 –
107 –
69 –
43 –
29 –

Control
P0-DG null

β-DG

212 –
107 –
69 –
43 –
29 –

Control
P0-DG null

C Immunofluorescence

Control

P0-DG null

D

600bp –
500bp –

Control sciatic nerve
Sciatic nerve
Brain
Skeletal muscle
Heart
Lung
Liver
Spleen
Kidney
Intestine

P0-DG null

E

Sciatic nerve

Brain

Skeletal muscle

Heart

Lung

Liver

Spleen

Kidney

Control
P0-DG null

Figure 1. Selective Loss of Dystroglycan from Peripheral Nerves of P0-DG Null Mice

(A) RT-PCR analysis of sciatic nerve shows loss of mRNA for DG in P0-DG null mice.
(B) Western blot reveals both α- and β-DG are lost in the sciatic nerve of P0-DG null mice.
(C) Immunofluorescent microscopic analysis demonstrates that the ring-like staining of β-DG is completely absent in the P0-DG null mice in spite of normal staining in the surrounding skeletal muscle.
(D) The recombination of floxed DG gene is detectable only in sciatic nerve.
(E) Western blot shows that β-DG is normally expressed in tissues other than sciatic nerve of P0-DG null mice. Littermates of $Dag1^{lox/lox}$ mice are used as controls.

in myelination. Moreover, peripheral nerve DG-protein complexes are disrupted and high-affinity laminin binding is reduced in the mutant mice. Finally, we demonstrate that DG normally colocalizes with ezrin-radixin-moesin (ERM) proteins in Schwann-cell microvilli, where it may contribute to the molecular architecture of the node of Ranvier. The loss of DG leads to disorganized Schwann cell microvilli and reduced nodal voltage-gated sodium (Na^+) channels. Taken together, these data indicate that DG plays important roles in myelination and Na^+ channel stabilization in peripheral nerve. We propose that the laminin-DG axis provides adhesive and/or signaling properties necessary for normal maintenance of the myelin sheath and that DG stabilizes Na^+ channels at the node of Ranvier by maintaining microvillus organization and mediating trans Schwann cell-axolemmal interactions.

Results

Generation of Mice Lacking Schwann Cell Dystroglycan

To ablate the DG gene (*Dag1*) selectively in Schwann cells, we used Cre-loxP methods (Gu et al., 1994). We mated the homozygous *Dag1^lox/lox^* mice (Cohn et al., 2002) with hemizygous mice for the P0 Cre transgene. The transgene is driven by regulatory sequences from the whole P0 gene, and Cre-recombinase is expressed selectively in Schwann cells beginning at embryonic day 14.5 (Feltri et al., 1999). The resultant heterozygous mice for *Dag1^lox^* carrying P0 Cre transgene (*Dag1^lox/wt^*/P0-Cre) were further mated with the homozygous *Dag1^lox/lox^* mice to produce *Dag1^lox/lox^*/P0-Cre (P0-DG null) mice. The P0-

DG null mice are born according to Mendelian ratio, grow normally, and are fertile.

The ablation of DG from peripheral nerves of 4-week-old P0-DG null mice was verified by reverse transcription PCR (Figure 1A), Western blot analysis (Figure 1B), and immunofluorescent microscopy (Figure 1C). The same result was obtained at postnatal days 1 and 7 (data not shown). Peripheral nerve selectivity of Cre-mediated recombination and β-DG ablation is shown by PCR (Figure 1D) and Western blot (Figure 1E).

Abnormal Myelination in P0-DG Null Mice

To examine if the disruption of DG affected peripheral nerve structure, we first evaluated crosssections from various nerves of P0-DG null mice by light microscopy. Sciatic nerves from P0-DG null mice at postnatal days 3, 7, and 14 exhibited numerous redundant myelin loops, represented primarily as comma-shaped myelin extensions (Figure 2B).

In adult mice from 2 to 24 months of age, myelin loops of a more irregular nature increased in number and developed into complex shapes. Indeed, numerous irregularly thickened or extensively folded myelin sheaths were observed in the older P0-DG null mice (Figures 2D and 2F). Teased fibers demonstrate that the excessive folding of myelin sheaths extends throughout the internodal segment (Figure 2H) and is not limited to the paranodal regions as is sometimes seen in control nerves. These abnormal myelin sheaths were observed to a similar degree in sciatic, tibial, sural, phrenic, caudal, and digital nerves from the mutant mice. An increase in the endoneurial space of older mutant mice is best demonstrated in phrenic nerves, which are strikingly
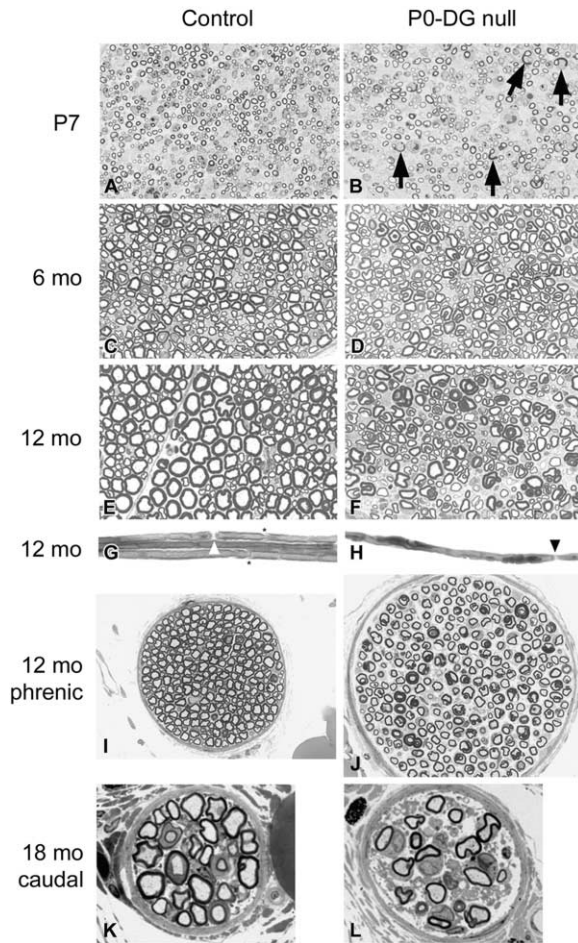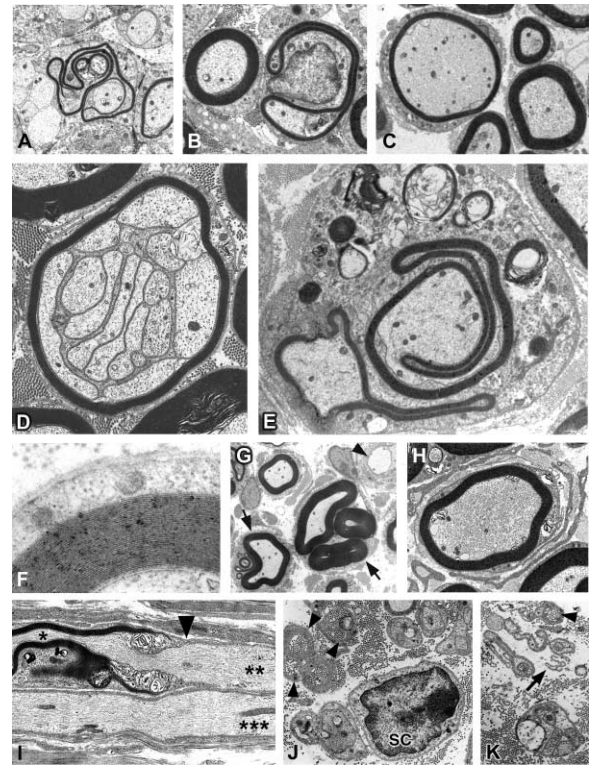
Figure 2. Abnormal Myelination in P0-DG Null Mice

Toluidine blue-stained epon sections of control (A, C, and E) and P0-DG null (B, D, and F) sciatic nerves are shown at the same magnification. Nerves from postnatal day 7 (P7) mutant mice contain elongated myelin loops, most commonly forming comma shapes (arrows in B). Extensively folded myelin sheaths increase with age in P0-DG null mice. Teased fibers from sciatic nerves of 12-month-old control (G) and P0-DG null (H) mice show that abnormal myelin folding is present along the entire internode. Arrowheads mark nodes of Ranvier and asterisks mark Schmidt-Lanterman incisures. Control (I) and P0-DG null (J) phrenic nerves from 12-month-old littermates show complex myelin folding similar to sciatic nerve and emphasize an increase in endoneurial space that results in a greatly enlarged nerve diameter in the mutant mice. Light microscopic evaluation of epon sections from caudal nerve twigs shows reduced numbers of myelinated axons in P0-DG null mice (L) as compared to age-matched controls (K).

Figure 3. Ultrastructural Abnormalities of Myelination in P0-DG Null Mice

Extremely long and sometimes circuitous myelin loops are present in postnatal day 3 (A) and postnatal day 7 (B) sciatic nerves from P0-DG null mice. The abnormal loop in (B) corresponds to the comma-shaped structures seen by light microscopy in Figure 2B. Abnormally thin myelin sheaths (upper left axon of C) are present in a minority of myelinated fibers from all ages and locations evaluated. Polyaxonal myelination is present in two forms: clusters of small axons surrounded by a common myelin sheath (D) and more than one myelinated axon within a common Schwann cell (E). Occasionally, axons extend a process inside the long myelin loops (right axon of E). Despite the abnormal myelin loops, myelin compaction (myelin periodicity) is normal and basal laminae are seen around all myelinating Schwann cells (F). Complex myelin loops are present in numerous myelinated fibers from 12-month-old mice (arrows in G). Features of demyelination/remyelination such as absence of myelin around a large axon (arrowhead in G) and onion bulb formation (H) are seen in 12-month-old mice. Segmental demyelination is more clearly evident in the longitudinal section of an older mouse (I) where a thin myelin sheath is present to the left of the node of Ranvier (single asterisk marks axon and arrowhead marks position of node), but no myelin is present to the right of the node (double asterisks). An adjacent axon is demyelinated (triple asterisks). Ultrastructural analysis verifies the loss of myelinated axons (J and K), characterized by empty Schwann cells (SC), collagen pockets (arrowheads), and redundant basal lamina (arrow).

enlarged (Figure 2J). Axonal loss occurs in aging mutant mice. Although variability of caudal nerve branching patterns and nerve fascicle size make the counting of absolute numbers of axons difficult, comparisons of similar sized nerve twigs showed a loss of myelinated fibers (Figures 2K and 2L).

Next, we performed electron microscopic analysis. In P0-DG null mice at postnatal days 3 and 7, many redundant myelin loops were observed (Figures 3A, 3B, and 3E). Interestingly, axon processes protrude into the myelin loops in some cases (Figure 3E). By 12 months, extensively folded myelin sheaths composed of multiple

external myelin loops were evident (Figure 3G). Similar loops protruding into the axons were also observed (data not shown). Only occasionally were hypomyelinated or demyelinated axons (Figures 3C, 3G, and 3I) and onion bulbs (Figure 3H) noted. Furthermore, polyaxonal myelination, in which a single myelin sheath wraps a cluster of small axons, was observed (Figure 3D). Rarely, two myelinated axons were present in the same Schwann cell (Figure 3E). The myelin compaction was normal and Schwann cell basal laminae were present

in the P0-DG null mice (Figure 3F). Myelinated axon loss in the oldest mice (Figure 2L) was substantiated by ultrastructural studies of caudal nerve twigs showing empty Schwann cells (bands of Bungner), collagen pockets, and strands of basal lamina not associated with cell processes (Figures 3J and 3K). These ultrastructural features of axonal loss were less commonly encountered in phrenic, sciatic, tibial, or sural nerves of the same mice (data not shown).

DG-Protein Complex Disruption in P0-DG Null Mice

To gain insight into the mechanism leading to abnormal myelin formation or maintenance in the P0-DG null mice, we examined whether components of the DG-protein complexes are retained in the peripheral nerve of P0-DG null mice by Western blot. In total homogenates of control sciatic nerve, β-sarcoglycan (SG), δ-SG, ε-SG, DP116, utrophin, DRP2, and L-periaxin were detected, but α-SG and γ-SG were not (Figure 4A, data for α-SG is not shown). This is consistent with previous reports (Saito et al., 1999; Imamura et al., 2000; Sherman et al., 2001). In addition, we observed that sarcospan, α-dystrobrevin 1, and α1-syntrophin, which are established DGC components in skeletal muscle, were also expressed in peripheral nerve (Figure 4A). In P0-DG null sciatic nerve, however, β-SG, δ-SG, ε-SG, sarcospan, DP116, α-dystrobrevin 1, and DRP2 were lost or severely reduced (Figure 4A). These results strongly suggest that these molecules form tight complexes with DG in peripheral nerve and that DG is essential for the stable expression of these proteins. The expression of utrophin, L-periaxin, and laminin α2, β1, and γ1 chains was not different from control, and α1-syntrophin was only mildly reduced in homogenates from P0-DG null mice (Figure 4A). In contrast, utrophin was absent from membrane preparations, while α1-syntrophin was only mildly reduced (Figure 4B). This suggests a major portion of Schwann cell α1-syntrophin is anchored at the membrane by molecules other than DG. β1 integrin, an alternate laminin receptor, appears unchanged in the mutant (Figures 4B and 4C). L-periaxin was not clearly detected in the membrane preparation of either control or mutant mice (data not shown); however, immunofluorescent analysis of crosssections (not shown) and teased fibers demonstrated normal L-periaxin staining in spite of decreased expression of DRP2 (Figure 4C). These data suggest that the localization of L-periaxin is not dependent upon DG or DRP2.

Abnormal Laminin Binding and Laminin Cluster Formation by Cultured Schwann Cells

The P0-DG null mice show marked morphological abnormalities in myelin sheaths that may be due to disrupted linkage between ECM and Schwann cell cytoskeleton. To examine this linkage, we first assessed laminin binding activity in the mutant peripheral nerve. Laminin binding was lost in blot overlay assays of P0-DG null peripheral nerve membrane fractions (Figure 5A). In a quantitative solid phase binding assay, the total laminin binding capacity in peripheral nerve membrane fractions was reduced by approximately 50% in P0-DG null mice (Figure 5B). Next, we established primary
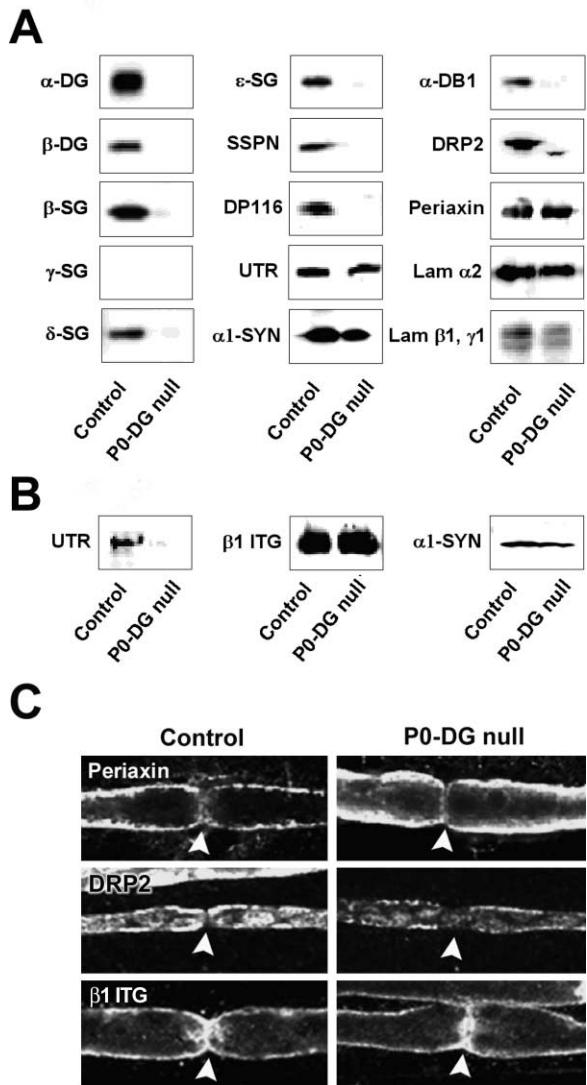
Figure 4. Abnormal DG-Protein Complex Expression in P0-DG Null Mice

(A) The total homogenate of sciatic nerve was subjected to Western blot. α- and β-DG, β-, δ-, and ε-sarcoglycan (SG), sarcospan (SSPN), DP116, utrophin (UTR), α-dystrobrevin (DB) 1, α1-syntrophin (SYN), dystrophin related protein 2 (DRP2), L-periaxin and laminin (Lam) α2, β1, and γ1 chains are expressed in control peripheral nerve, while γ-SG is not. In the mutant, β-, δ-, and ε-sarcoglycan (SG), sarcospan (SSPN), DP116, α-DB 1, and DRP2 are not detected or are severely reduced. L-periaxin is detected normally in the mutant nerves.

(B) Utrophin is not detected in membrane fractions from P0-DG null, while α1-syntrophin is observed in both control and the mutant. β1 integrin (β1 ITG) appears normal in the mutant nerves.

(C) In teased fibers, expression and localization of L-periaxin and β1 integrin are normal, whereas expression of DRP2 is reduced in P0-DG null mice (arrowheads mark nodes of Ranvier).

Schwann cell cultures to ask if the ablation of DG affected laminin clustering or morphogenesis of Schwann cells in vitro. Exogenous laminin formed plaque-like clusters on the control Schwann cell surface that colocalized with immunoreactive α-DG (Figure 5C). In contrast, no laminin clusters were observed on the mutant
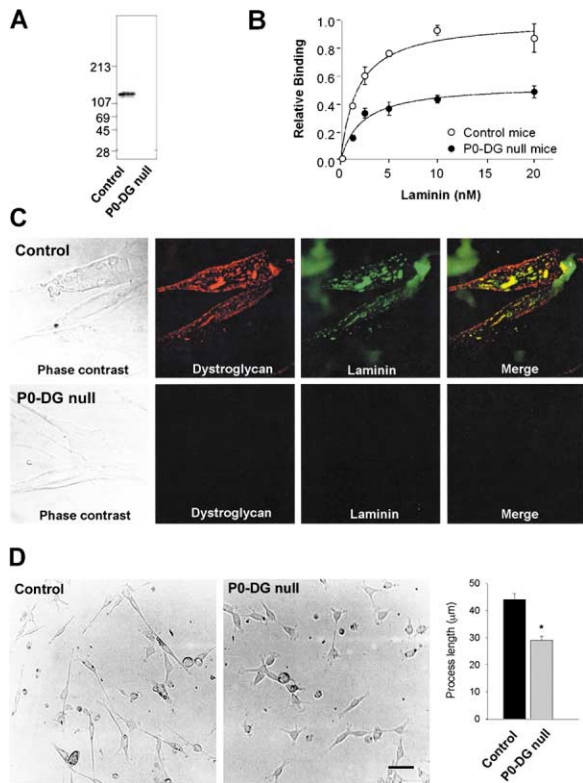
Figure 5. Abnormalities in Laminin Binding, Clustering, and Schwann Cells Process of P0-DG Null Mice

(A) Laminin blot overlay assay shows that laminin binding is absent in membrane fractions from P0-DG null mice.
(B) Solid phase binding assay reveals that laminin binding capacity is greatly reduced in P0-DG null mice. When the maximum binding of control is adjusted to 1, the maximum binding of P0-DG null mice is 0.54. Kd for control and the mutant is 1.72 nM and 2.15 nM, respectively.
(C) Laminin cluster formation colocalizes with immunoreactive α-DG on the control Schwann cells; however, laminin clusters are not observed on the mutant Schwann cells.
(D) Processes of Schwann cells cultured from mutant mice are shorter than those of control mice. Bar indicates 50 μm. The mean process length for control and P0-DG null are 44.0 $\pm$ 26.7 μm (n = 154) and 29.1 $\pm$ 15.7 μm (n = 125), respectively (*p < 0.001).

Figure 6. Neurological Dysfunction in P0-DG Null Mice

(A) In a protocol of step-wise increases in rotorod speed, P0-DG null mice (n = 9) improved significantly less than littermate control mice (n = 9) (one-tailed permutation probability, p = 0.0157).
(B) In an accelerating rotorod protocol, the same P0-DG null mice remained on the rod a significantly shorter period of time than the control mice (p = 0.0001).
(C) The responses of P0-DG null mice and control littermates to heat (n = 9 for the mutant and n = 10 for control) and mechanical stimuli (n = 10 for both the mutant and control) were measured. There was a significant increase in the withdrawal latency to higher intensity, but not lower intensity, heat in P0-DG null mice (*p < 0.05).
(D) There was a significantly increased number of withdrawals to all forces of stimuli in P0-DG null mice (*p < 0.01). This increase in the number of withdrawals was significantly reduced by 10 mg/kg i.p. of morphine (#p < 0.05).
(E) Shown here are representative oscilloscope tracings from control and P0-DG null littermates (CMAP, compound muscle action potential; NAP, nerve action potential); numerical data is in Table 1.

Schwann cells (Figure 5C). This disruption in laminin binding may affect Schwann cell morphogenesis since Schwann cells from P0-DG null mice cultured on laminin-coated plates had shorter processes compared to those from control mice (Figure 5D; p < 0.001).

Neurologic Abnormalities in P0-DG Null Mice

The P0-DG null mice are indistinguishable by visual observation from their control littermates until approximately 1 year of age, when a subtle tremor that is accentuated with movement is noted. In addition, escape response from light finger stroke is less pronounced and slower in P0-DG null mice than in control mice. To quantitatively evaluate neurologic dysfunction in the mice, we performed rotorod testing in 14- to 18-month-old animals. During pretrial rotorod training, P0-DG null mice had a greater number of falls than controls (median number of falls 11 versus 1; one-tailed permutation prob-
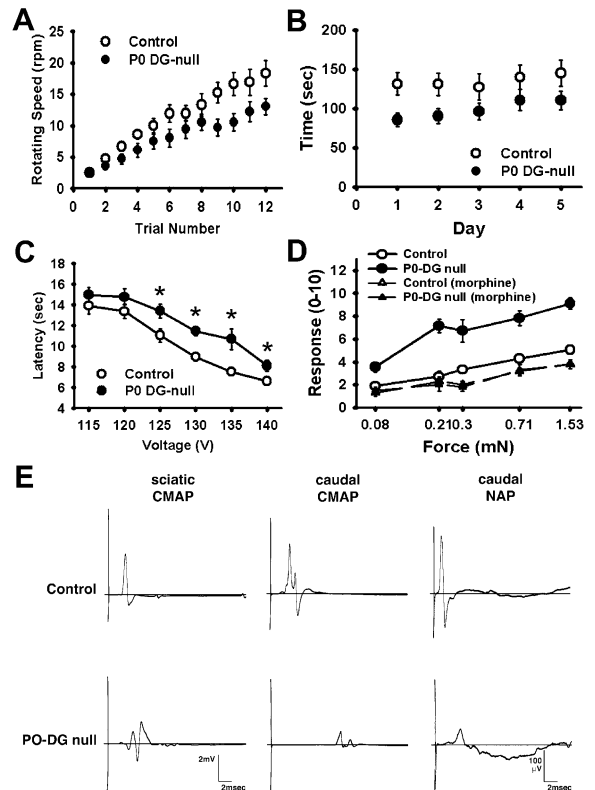
ability, p = 0.0007) and a shorter latency to first fall (mean latency of 38 s versus 91 s; one-tailed permutation probability, p = 0.0004). Data from the trial of step-wise increases in rotorod speed were evaluated in a number of ways. At the end of the four-day trial, P0-DG null mice attained a lower average rotorod speed than controls, 13.1 rpm versus 18.3 rpm (one-tailed permutation probability, p = 0.016) (Figure 6A). Furthermore, DG null mice were delayed in reaching the first step-up in rotorod speed (one-tailed permutation probability, p = 0.039) and were less likely to be promoted to higher rotorod speeds during the trial (one-tailed permutation probability, p = 0.008). Testing mice on the accelerating rotorod also demonstrated statistically poorer performance by P0-DG null mice (Figure 6B; p < 0.0001).

We also asked if the P0-DG null mice have sensory

Table 1. Nerve Conduction Velocities and Action Potential Amplitudes Are Reduced in P0-DG Null Mice

	Control	P0-DG Null
NAP in Caudal Nerve		
Conduction velocity (m/s)		
Proximal stimulation	33.5 ± 2.1	6.9 ± 1.8*
Distal stimulation	34.3 ± 1.0	7.8 ± 2.1*
Amplitude μ(V)		
Proximal stimulation	82.4 ± 11.2	9.4 ± 4.1*
Distal stimulation	166.4 ± 25.2	14.5 ± 4.3*
CMAP in Caudal Nerve		
Conduction velocity (m/s)	29.6 ± 1.5	6.0 ± 1.0*
Amplitude (mV)		
Proximal stimulation	3.0 ± 0.2	0.8 ± 0.2*
Distal stimulation	5.0 ± 0.7	0.8 ± 0.1*
CMAP in Sciatic-Tibial Nerve		
Conduction velocity (m/s)	39.4 ± 2.3	29.0 ± 1.3*
Amplitude (mV)		
Proximal stimulation	6.8 ± 0.9	2.8 ± 0.6*
Distal stimulation	7.5 ± 1.0	2.9 ± 0.4*
SNAP in Digital Nerve		
Conduction velocity (m/s)	33.7 ± 1.4	14.9 ± 1.1*
Amplitude μ(V)	20.2 ± 2.1	9.5 ± 1.8*

Electrophysiological recordings are from 14- to 15-month-old P0-DG null mice and littermate controls. All data are expressed as mean ± SE. Sample size is n = 5 for both P0-DG null and control mice.
* $p < 0.005$; NAP, nerve action potential; CMAP, compound muscular action potential; SNAP, sensory nerve action potential.

dysfunction by testing the withdrawal response to heat and mechanical stimuli. There was a significant increase in the withdrawal latency to heat with higher intensities of stimulation, but not lower intensities, in P0-DG null mice of 12 to 19 months of age when compared to control littermates (Figure 6C). Since higher intensities of stimulation activate Aδ nociceptors while lower intensities activate C-nociceptors (Yeomans and Proudfit, 1996), it is possible that there is a selective loss of Aδ nociceptor activity in P0-DG null mice. There was a significant increase in the number of withdrawals to von Frey filaments of all bending forces tested in the mutant mice (Figure 6D). The increase in withdrawals was eliminated by systemic morphine (Figure 6D), indicating P0-DG null mice are hyperalgesic to mechanical stimuli.

Nerve Conduction Impairment in P0-DG Null Mice
Due to the severity of myelin sheath pathology and neurologic dysfunction, we investigated nerve conduction in the P0-DG null mice. At 15 months of age, changes characteristic of demyelination were seen in several nerves (Table 1). In addition to significantly increased latency and temporal dispersions of both nerve and compound muscle action potentials (Figure 6E), the conduction velocity (CV) in caudal nerve was decreased to approximately 20% of control and amplitude was decreased to 10% of control ($p << 0.005$). The CV in the sciatic-tibial nerve was altered to a lesser degree, but also showed significant slowing (74% of control; $p < 0.005$); sciatic-tibial amplitude was reduced to ∼40% of control ($p < 0.005$). These data provide clear evidence

of electrophysiological abnormalities in both motor and sensory nerves in P0-DG null mice. Testing of a smaller group of P0-DG null mice at 6 months of age (n = 4) revealed a pattern of nerve conduction changes similar to those at 15 months, but the slowing and amplitude changes were less severe (e.g., caudal nerve NAP conduction velocity was 12.1 ± 1.8 m/s). This indicates that conduction abnormalities (1) occur in young adult mice and (2) progress in severity with age.

Expression of Nodal Proteins and Reduction of Na^+ Channels in P0-DG Null Mice
Because the severity of the nerve conduction abnormalities appeared to exceed the degree of classic demyelination/remyelination pathology, immunofluorescence analysis was undertaken to determine if there might be abnormal localization of nodal proteins that could explain the profoundly reduced conduction velocities and amplitudes. As shown in Figure 7A, DG localizes not only in the Schwann cell outer membranes but also at the nodes of Ranvier. Double staining experiments of crosssections (not shown) and teased fibers further revealed that DG colocalizes with moesin rather than ankyrin-G, suggesting that DG is expressed in the microvilli of Schwann cells but not in the axonal membrane of the nodal region (Figure 7A). In the mutant nerves, the pattern and intensity of staining for ankyrin-G, moesin, E-cadherin, neurofascin (the antibody recognizes both neurofascin 155 and 186), and the juxtaparanodal protein caspr2 were indistinguishable from those in control. In sharp contrast to the normal expression of this broad array of nodal proteins, Na^+ channel staining was reduced at mutant nodes of Ranvier or dispersed laterally along a broad region of the axon instead of colocalizing in a narrow band with ankyrin-G (Figure 7B). These abnormalities of Na^+ channel expression were noted in both frozen crosssections and teased fibers. Quantitation of abnormal nodes of Ranvier in teased fibers showed that >90% had reduced Na^+ channel immunoreactivity, while Na^+ channels were dispersed laterally along the axon in another 7% (Table 2). Comparable abnormal staining was seen with several pan Na^+ channel, $Na_v1.6$ (Figure 7B, B13), and β2 subunit (Figure 7B, B14) antibodies. No $Na_v1.2$ staining was detected. In contrast, K^+ channels are not mislocalized at the node of Ranvier. Mutant nerve fibers had the expected paranodal gap between the node itself and immunoreactive K^+ channels in the juxtaparanodal region (data not shown). Neurofascin/K^+ channel dual labeling confirmed that there has been no medial displacement of K^+ channels toward the nodes (Figure 7B, B15). Western blots of peripheral nerve homogenates showed no appreciable loss of total Na^+ channel protein (data not shown), suggesting that the abnormality is solely, or at least primarily, one of defective channel stabilization.

Ultrastructural Abnormalities in P0-DG Null Nodes of Ranvier
In order to determine if structural abnormalities might underlie or accompany the changes in Na^+ channel clustering, electron microscopic studies analyzed transverse and longitudinal sections of sciatic nerves from P0-DG null and littermate controls between 3 and 24
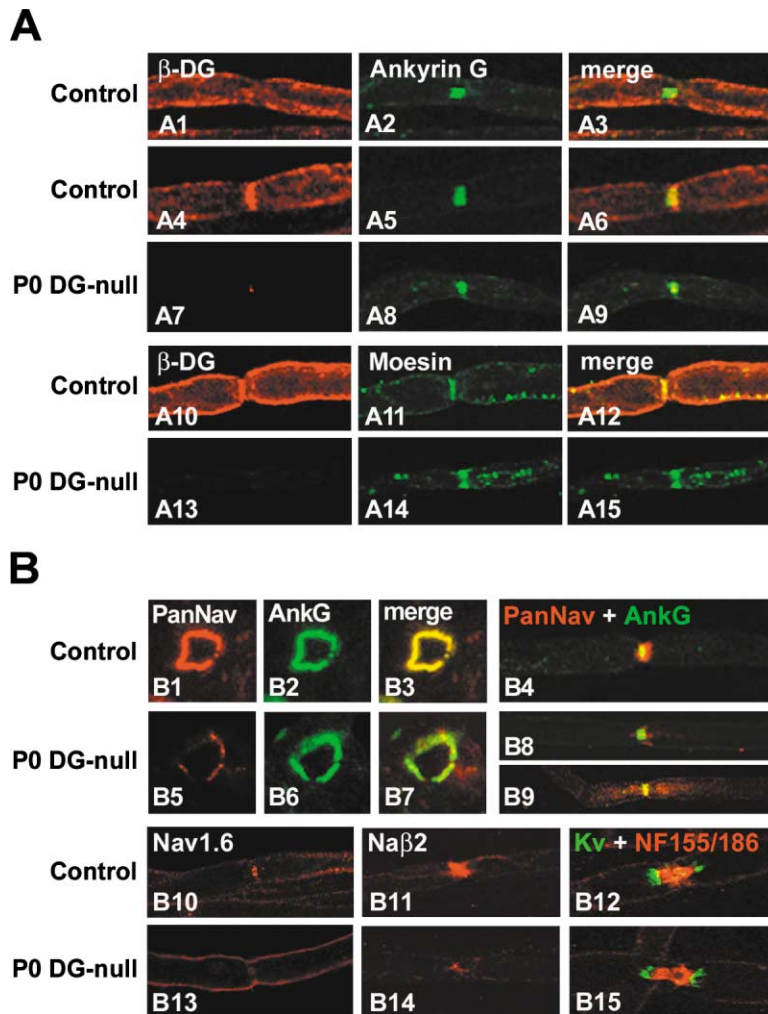
A

B

Figure 7. Localization of Dystroglycan and Nodal Proteins in Teased Fibers

(A) Immunofluorescent analysis of teased fibers from sciatic nerves of mice between 2 weeks and 18 months of age demonstrates that DG localizes at the nodes of Ranvier as well as the Schwann cell outer membrane. Dual staining experiments reveal that DG colocalizes with moesin rather than ankyrin-G. Panels A1–A3 are from a single confocal level and show almost no overlap between DG and ankyrin-G at the node. Panels A4–A6 are from a Z series stack. The merged image (A6) shows partial overlap of immunofluorescence only over the axon, while only DG signal is seen at the outer margins of the node in the area corresponding to the nodal gap occupied by Schwann cell microvilli. In contrast, DG and moesin immunofluorescence overlap entirely in a single confocal level (A12).

(B) Immunofluorescent microscopy of frozen crosssections and teased fibers demonstrates that Na^+ channels and ankyrin-G are strongly expressed and colocalized in control nodes of Ranvier (B1–B4). However, expression of Na^+ channels at the node is reduced in P0-DG null mice (B5–B8). In some nodes from mutant mice, Na^+ channel immunoreactivity was dispersed laterally along the axon (B9). Reduced Na^+ channel clustering at the nodes of P0-DG null mice is confirmed by immunolabeling with antibodies specific for $Na_v1.6$ (B13) and Na^+ channel $\beta 2$ subunit (B14). Meanwhile, the expression of K^+ channels ($K_v1.1$) and neurofascins 155 and 186 are not altered (B15).

months of age. Several structures of the paranodal region appear normal or nearly normal in P0-DG null mice (Figures 8A and 8B), including lateral loops, septate axoglial junctions, and autotypic adherens junctions (Fannon et al., 1995). However, structures at the node itself are abnormal. Schwann cell microvilli normally have a relatively regular, radial arrangement around the centrally located axon (Figures 8C and 8G; Berthold and Rydmark, 1983). In P0-DG null nerves, there are variable degrees of microvillus disorganization and blunting (Figures 8D–8F). At some nodes there are no discernable

microvilli, and the node is simply capped by flat Schwann cell processes and their associated basal lamina (Figure 8A). While microvillus lengths were not measured, the nodal gap height (distance from axolemma to basal lamina) is less in P0-DG null nodes. Representative examples of this are illustrated in Figures 8A and 8C–8E, where the nodal axon diameters are quite similar (diameters range from 1.8 to 2.2 μm). Despite the uniform axon size, the nodal gap height in the control varies from 0.4 to 1.2 μm (Figure 8C), while the nodal gap heights in the P0-DG null nerves are 0.2 μm in Figure 8A, 0.4 to

Table 2. Abnormal Na^+ Channel Immunofluorescence in P0-DG Null Sciatic Nerves

	Normal	Reduced[a]	Diffuse[b]	Total[c]
Control	n = 68 (92%)	n = 6 (8%)	n = 0 (0%)	n = 74
DG-null	n = 1 (1%)	n = 85 (92%)	n = 6 (7%)	n = 92

Polyclonal pan-Na^+ channel antibodies were used to assess Na^+ channel expression in nodes of Ranvier identified as ankyrin-G-positive regions of axons in teased fiber preparations (see Figure 7). Mice ranged in age from 16 days to 78 weeks. n = 6 for control mice; n = 9 for P0-DG null mice.
[a] Nodes scored as reduced staining had less immunoreactivity at the node of Ranvier without any staining in the adjacent axon (see Figure 7, panel B8).
[b] Nodes scored as diffuse staining had less immunoreactivity at the node of Ranvier in addition to dispersion of immunoreactivity along the adjacent axon (see Figure 7, panel B9).
[c] Numbers in this column are the total number of nodes of Ranvier evaluated.
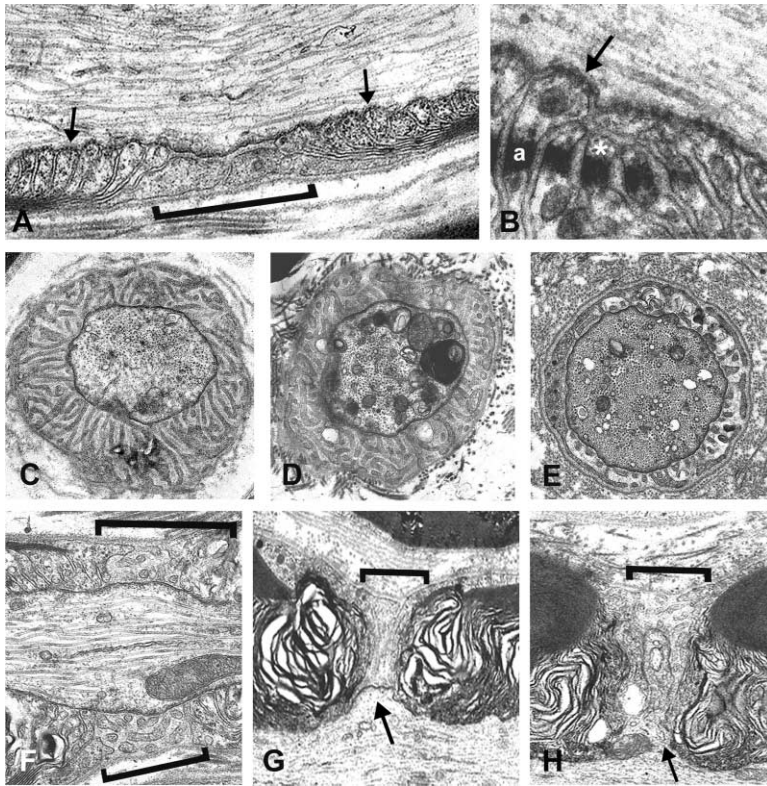
Figure 8. Ultrastructure of Nodal Structures

Several structures of the paranodal region appear normal or nearly normal in P0-DG null mice, including lateral loops with septate axoglial junctions (arrows in A and B) and autotypic adherens junctions (lowercase "a" in B). A small number of lateral loops fail to contact the axolemma in some myelinated fibers (asterisk in B). Schwann cell microvilli normally have a relatively regular, radial arrangement around the centrally located axon (control crosssection in panel C; control longitudinal section in panel G, bracket marks region of nodal gap). However, in P0-DG null nerves, there are variable degrees of microvillus disorganization and blunting (crosssections in D and E; longitudinal sections in F and H, brackets mark regions of nodal gaps). There are no microvilli at occasional nodes of Ranvier (bracket in A). Some DG null nodes have long lateral axonal protrusions (or spines) like the one shown in panel H (arrow at neck of spine). Arrow marks a normal axonal dome in a control, panel G.

0.7 μm in Figure 8D and 0.2 to 0.5 μm in Figure 8E. The reduced nodal gap height is likely the result of Schwann cell microvillus abnormalities in mutant nerves. Axonal abnormalities are also present in P0-DG null nodes where there commonly are accentuations of normal lateral protrusions termed domes or spines by Berthold and Rydmark (1983) (data not shown). Occasionally, elongated axonal protrusions (or spines) are present in the nodal segments of P0-DG null axons (Figure 8H).

Discussion

We demonstrate a progressive neuropathy in mice in which DG is selectively ablated from Schwann cells. The absence of DG is sufficient to cause abnormalities in structure and function that include mildly impaired radial sorting of axons, dysmyelination, demyelination, axonal loss, and aberrant nerve conduction. Several components of Schwann cell DG protein complexes are lost and laminin binding is disrupted. Moreover, DG normally colocalizes with moesin, an ERM protein found in Schwann cell microvilli (Melendez-Vasquez et al., 2001; Scherer et al., 2001), and the loss of DG leads to disorganization of microvilli and reduction of immunoreactive Na+ channels at nodes of Ranvier. Taken together, our findings implicate DG in myelin integrity and in node of Ranvier structure and function.

Distinct Roles for Dystroglycan and β1 Integrin in Radial Sorting and Myelination

Myelinating Schwann cells express α6β1 and α6β4 integrin in addition to DG; all are putative laminin receptors (Previtali et al., 2001). While myelination proceeds normally in the absence of β4 integrin (Frei et al., 1999), mice lacking β1 integrin in Schwann cells show a major abnormality in radial sorting (Feltri et al., 2002). By this process, immature Schwann cells segregate axons and attain a 1:1 relationship with larger caliber axons before forming myelin sheaths. Impairment of radial sorting is also the hallmark of the neuropathy in dy/dy mice in which laminin 2 is deficient (Bradley and Jenkison, 1973, 1975; Jaros and Bradley, 1979).

In sharp contrast to β1 integrin null mice, most Schwann cells in P0-DG null mice pass through the promyelination stage and myelinate axons in the appropriate 1:1 relationship. However, a small amount of polyaxonal myelination, another manifestation of abnormal radial sorting, is seen in P0-DG null mice. But even when polyaxonal myelination occurs in P0-DG null mice, the process of ensheathing seems not to be arrested as is the case in β1 integrin null mice; instead, myelination proceeds incorrectly. A similar degree of polyaxonal myelination has been observed in dy/dy mice (Okada et al., 1977) and in leprous neuropathy patients and animal models (Shetty, 1995). *M. leprae* bind to α-DG in conjunction with the G domain of laminin α2 in order to target Schwann cells (Rambukkana et al., 1998). These observations strongly suggest that β1-integrin plays a greater role than DG in the sorting of axons in the promyelination stage, while DG plays a more critical role in organized myelin formation and its maintenance at later stages.

Neuropathy with Abnormal Myelin Folding in P0-DG Null Mice

The myelin pathology manifesting as abnormal folding is present in two different ages of P0-DG null mice. Early postnatal P0-DG null mice have numerous elongated

(redundant) myelin loops that may reflect problems in the initial formation of myelin sheaths. Interestingly, axon processes were observed to extend into the myelin loops in some cases. This aberrant axon morphology suggests that the loss of DG may affect axonal structure in addition to myelin sheaths.

In older mice, a mild degree of demyelination/remyelination (hypomyelination, naked axons, and onion bulbs) is noted in the mutants. However, a more prominent abnormality is the presence of extensively folded myelin sheaths. The abnormal myelin sheaths in these older mice may be pathogenetically distinct from the redundant myelin loops of postnatal mice. Their bizarre shapes are distinct from tomacula that are seen in hereditary neuropathy with liability to pressure palsies (Chance, 1999). The extensive myelin folding observed in P0-DG null mice more closely resembles at least one form of autosomal recessive hereditary neuropathy, e.g., Charcot-Marie-Tooth disease type 4F (Guilbot et al., 2001).

We demonstrated that laminin binding activity is substantially reduced in the peripheral nerve of P0-DG null mice, and we observed the absence of laminin cluster formation on P0-DG null Schwann cells. There was also altered process formation of the mutant Schwann cells cultured on laminin-coated plates. This suggests that the laminin-DG interactions are important for normal Schwann cell morphology. Tsiper and Yurchenco (2002) have shown that basement membrane formation in cultured Schwann cells involves the DG-utrophin linkage to laminin.

However, the redundant myelin loops and extensive folding observed in P0-DG null mice are not reported in dy/dy mice. This indicates that the abnormal folding may be independent of disruption of the DG-laminin linkage itself. Instead, it is possible that the dissociation of cytoplasmic protein linkages with DG (in other words, disruption of DG complexes) may lead to the unique dysmyelination phenotype of P0-DG null mice. The loss of sarcoglycans and sarcospan may have little impact upon the phenotype, because β-SG-deficient mice in which the entire sarcoglycan-sarcospan complex is lost (Durbeej et al., 2000) have revealed no histopathologic evidence of peripheral neuropathy in preliminary studies (data not shown). In contrast, the loss of DRP2 may play an important role. L-periaxin-deficient mice as well as patients with periaxin mutations (CMT4F) exhibit folded myelin sheaths and sensory dysfunction similar to the P0-DG null mice (Gillespie et al., 2000; Boerkoel et al., 2001; Guilbot et al., 2001). DRP2 is lost concomitantly in the L-periaxin-deficient mice, although DG is normally localized to Schwann cell membranes (Sherman et al., 2001). In P0-DG null mice, DRP2 is severely reduced, while L-periaxin appears to be normally expressed. Therefore, DRP2 may be a key molecule leading to the folded myelin formation in these different lines of mutant mice.

Na$^+$ Channel Reduction and Structural Abnormalities at Nodes of Ranvier

The profound abnormalities in peripheral nerve conduction of P0-DG null mice prompted us to presume that saltatory conduction could be defective because of abnormalities in the node of Ranvier. Myelinated fibers are organized into distinct nodal, paranodal, juxtaparanodal, and internodal domains. Na$^+$ channels, ankyrin-G, NrCAM, and neurofascin 186 colocalize at the node, while Caspr, contactin, and neurofascin 155 are enriched in the paranode and Caspr2 and K$^+$ channels are concentrated in the juxtaparanode (Peles and Salzer, 2000; Rasband and Trimmer, 2001; Scherer and Arroyo, 2002). Although a previous study suggested that DG was not present at nodes of Ranvier (Yamada et al., 1994), dual immunofluorescence shown here demonstrated that DG normally colocalizes with moesin, an ERM protein present in Schwann cell microvilli (Melendez-Vasquez et al., 2001; Scherer et al., 2001). With the loss of DG, Na$^+$ channel expression at the nodes is selectively reduced or dispersed along the axon. It has been shown that the formation of nodes of Ranvier in peripheral nerve requires contact-dependent signals from the Schwann cells (Ching et al., 1999). Clustering of neurofascin 186 (NF186) and NrCAM at developing nodal axolemma precedes those of Na$^+$ channels and ankyrin-G; thus, it is proposed that NF186 and NrCAM have heterophilic interaction with unknown molecules on the microvilli (Peles and Salzer, 2000). On the other hand, ERM proteins, which act as a linker connecting plasma membrane proteins and actin cytoskeleton, are localized at the Schwann cell microvilli that associate with ankyrin-G and Na$^+$ channel clusters in developing nodes (Melendez-Vasquez et al., 2001; Scherer et al., 2001). Therefore, it is intriguing to speculate that DG is scaffolded by ERM proteins at the microvilli and mediates the interaction between Schwann cells and the nodal axonal membrane. Sodium channel β subunit and neurofascin possess extracellular immunoglobulin-like domains and bind each other in *cis* through these domains (Ratcliffe et al., 2001). It is of particular interest to note that DG also has an extracellular immunoglobulin-like domain (Bozic et al., 1998). Thus, DG in the Schwann cell microvilli may interact with this nodal protein complex in *trans*, and this interaction may be necessary for the stable localization of Na$^+$ channels at the node.

Structural abnormalities observed at nodes of Ranvier also support a role for DG in this location. Paranodal structures, particularly septate axoglial junctions, appear to be critical for establishing normal Na$^+$ and K$^+$ channel localization during development, and several mouse mutants with abnormalities in paranodal architecture have displaced K$^+$ channels (Dupree et al., 1999; Boyle et al., 2001; Bhat et al., 2001; Ishibashi et al., 2002). The paranodal region in P0-DG null mice, however, is ultrastructurally essentially normal, and several paranodal and juxtaparanodal proteins (including K$^+$ channels) are normally localized. In contrast, the nodal domain architecture in DG mutant mice is disrupted: Schwann cell microvilli are disorganized and blunted to varying degrees and axons occasionally display accentuated lateral protrusions forming spines. These findings suggest that DG plays a role in maintaining nodal ultrastructure and that its absence leads to disruption of interactions between adjacent microvilli, between microvilli and the nodal axolemma, or both. Furthermore, nodal disorganization may be causally related to the reduction in Na$^+$ channel density and the profound slowing of NCV observed in P0-DG null mice.

Interruptions in DG-laminin linkage may also underlie these nodal abnormalities. Structural changes similar to

DG null nodes of Ranvier have previously been reported in dy/dy (Bradley et al., 1977; Jaros and Bradley, 1979) and dy^{3K}/dy^{3K} (Nakagawa et al., 2001) mice.

In conclusion, we have demonstrated that DG plays an important role in myelin sheath formation/maintenance, nodal structure, and Na$^+$ channel clustering in peripheral nerve. We propose that DG mediates these roles through at least two distinct interactions. First, there is a laminin-DG-DRP2/DP116/utrophin axis connecting the Schwann cell cytoskeleton to the ECM; disruption of these linkages may lead to CMT4F, leprous neuropathy, and neuropathies associated with muscular dystrophy. Second, we believe that DG contributes to trans interactions between Schwann cell microvilli and the nodal axolemma; disruption of these interactions is likely to contribute to the nerve conduction slowing in a similar array of neuropathic conditions.

Experimental Procedures

Generation of Floxed Dystroglycan Mice
The design of the floxed DG targeting construct has been reported previously (Moore et al., 2002; Cohn et al., 2002).

Polymerase Chain Reaction (PCR)
RT-PCR was carried out on total RNA isolated from sciatic nerve using RNAzolB (Tel-Test). Gene-specific sense primer (5′-GCTCAT TTCGAGTGAGCATTCC-3′) and antisense primer (5′-CTAGTTTC CAGGACAGGAGA-3′) were designed. Reverse transcription and PCR were performed with SuperScript One Step RT-PCR with PLAT-INUM Taq (GIBCO-BRL). DNA was isolated from each tissue by proteinase K digestion and ethanol precipitation. Gene-specific sense primer (5′-CGAACACTGAGTTCATCC-3′) and antisense primer (5′-CAACTGCTGCATCTCTAC-3′) were designed to anneal to the intronic sequences flanking exon 2, which allow amplification of a 585 bp fragment only when exon 2 and the neo cassette are excised by Cre recombinase.

Histology, Immunofluorescence, and Electron Microscopy
Histopathological studies were performed on P0-DG null and age-matched, littermate control mice between the ages of postnatal day 3 and 24 months using standard frozen section, epon section, teased fiber, and electron microscopic techniques. Between 3 and 10 P0-DG null and control mice were evaluated at each time point presented in the paper.

Antibodies
Affinity-purified polyclonal antibodies were utilized for β-DG (Ibragh-imov-Beskrovnaya et al., 1992), laminin α2 chain (Allamand et al., 1997), neurofascin (Tait et al., 2000), δ-SG, ε-SG, sarcospan, and β-SG (Duclos et al., 1998). DRP2 and periaxin antibodies were described previously (Sherman et al., 2001). The monoclonal antibody IIH6 was used for α-DG (Ervasti and Campbell, 1993). Anti-laminin α 1 chain and anti-α1-syntrophin were kind gifts from Dr. Lydia Sorokin and Stanley Froehner, respectively. Monoclonal antibodies against α-SG, Ad1/20A6, γ-SG, and 35DAG/21B5 were generated in collaboration with L.V.B. Anderson. Rabbit polyclonal antibody was generated against the C-terminal 12 amino acids (CCPN VPSRPQAM) of utrophin and affinity purified. Rabbit polyclonal anti-laminin, monoclonal anti-dystrophin (MANDRA-1), and pan-Na$^+$ channel antibodies were from Sigma. Monoclonal anti-dystrobrevin, clone 23, and anti-moesin were from Transduction Laboratories. Rabbit polyclonal anti-Caspr2 and monoclonal anti-ankyrin-G were from Alomone Labs, Zymed, and Boehringer Mannheim, respectively. Rabbit polyclonal anti pan-Na$^+$ channel, monoclonal anti Na$_v$1.2, Na$_v$1.6, and Naβ2, and monoclonal anti-β1 integrin were from Chemicon. James Trimmer kindly provided monoclonal Na$_v$1.2, Na$_v$1.6, and pan Na$_v$ antibodies. Anti-K$_v$1.1 α subunit, clone K20/78, was from Upstate Biotechnology. Peroxidase-conjugated secondary antibodies were purchased from Vector. Cy3- and FITC-conju-gated secondary antibodies were from Jackson ImmunoResearch, while AlexaFluor tagged secondary antibodies were from Molecular Probes.

Rotorod Testing
Rotorod performance was tested in P0-DG null and littermate control mice, 14 to 18 months of age, using a protocol modified from Thouvarecq et al. (2001). The day before formal testing, mice were subjected to three training trials at a fixed rotorod speed of 2.5 rpm. The latency to first fall and the total number of falls during each 120 s training session were recorded. Mice were then subjected to a protocol of step-wise increases in rotorod speed that consisted of a series of three trials per day over four consecutive days. All mice started at 2.5 rpm and were allowed to walk on the rotorod for up to 180 s. After each successful trial, the speed was increased by 2.5 rpm for the next trial. After each unsuccessful trial, the speed was decreased by 2.5 rpm for the next trial. The following week, mice were tested on five consecutive days using an accelerating rotorod protocol (0 to 40 rpm over 4 min). The latency before falling was recorded for each mouse. Data from the pretrial training and step-wise increase trial were statistically evaluated by permutation analyses using Resampling Stats® software, while data from the accelerating rod trial were evaluated using the MIXED procedure in SAS(r) to fit a mixed ANOVA model.

Behavioral Test for Pain Stimuli
Responses of P0-DG null mice and control littermates of 12 to 19 months of age to heat and mechanical stimuli were tested. First, the latency to withdrawal from heat stimuli of different intensities was determined. Three trials per intensity were averaged for each animal. Next, von Frey filaments were applied to the plantar surface of the paw to assess mechanical hyperalgesia. The number of withdrawals out of 10 tests was assessed for each bending force. Morphine, 10 mg/kg, i.p. (Sigma), was given to 5 mutant and 5 control mice, and responses to von Frey filaments were retested starting 30 min after injection (Wacnik et al., 2001). Data were analyzed with a one-way ANOVA for each heat intensity or von Frey filament. Data for morphine were analyzed with a paired t test for each von Frey filament before and after treatment with morphine.

Nerve Conduction
Nerve conduction studies were performed as described previously (Low et al., 1984). We measured the amplitude of muscle compound action potential (MCAP) in sciatic-tibial and caudal nerves and nerve action potential (NAP) in digital and caudal nerves. The MCAP was recorded from the dorsum of the hindpaw while stimulating at the level of the sciatic notch and ankle for sciatic-tibial nerve. For caudal nerve, the MCAP and NAP were recorded from the tail while stimulating at two proximal sites. The NAP was recorded from the ankle while stimulating digital nerve at the digit tip. Recordings were done at 35°C. The signals were analyzed offline using a digital oscilloscope (Nicolet Instruments, Madison, WI). Statistical comparisons were performed by t test.

Schwann Cell Culture
Schwann cell culture was performed as reported previously (Komiyama et al., 1991). Crush injury was made to sciatic nerves of 8- to 12-week-old P0-DG null and control mice. Two weeks after surgery, Schwann cells were dissociated from chopped distal nerve segments using 1.25 U/ml dispase II (Roche), 0.05% collagenase, type 1 (Worthington), and 0.1% hyaluronidase (Sigma) overnight at 37°C. The cells were plated at a density of 3×10^4 cells/well onto laminin-coated 24-well plates. Cultures were fed with DMEM, 10% FBS, 1000 U/ml penicillin, 1000 μg/ml streptomycin, and 2 mM L-gluta-mine. The process length of Schwann cells was measured 5 days after plating. At least 125 processes were measured and statistical significance was evaluated using t test. A laminin cluster assay was performed as previously described (Henry et al., 2001).

Biochemical Analysis
For biochemical analysis, tissues were isolated and disrupted with a polytron followed by Dounce homogenization in 50 mM Tris-HCl (pH 7.4), 150 mM NaCl, 0.6 μg/ml Pepstatin A, 0.5 μg/ml leupeptin,

0.5 μg/ml aprotinin, 0.75 mM benzamidine, 0.1 mM PMSF, 0.4 μg/ml calpain inhibitor 1, 0.4 μg/ml calpeptin. After briefly spinning down debris, the homogenate was applied to 3%–12% SDS-PAGE and resolved under reducing condition. Membranes from peripheral nerve were prepared and washed with KCl as described previously (Ohlendieck and Campbell, 1991). Western blotting, laminin blot overlay, and solid phase binding assays were described previously (Durbeej et al., 2000; Saito et al., 1999; Michele et al., 2002; Henry et al., 2001). Mouse EHS laminin, primarily laminin 1, was used in these assays (Biomedical Technologies, Inc.).

References

Allamand, V., Sunada, Y., Salih, M.A., Straub, V., Ozo, C.O., Al-Turaiki, M.H., Akbar, M., Kolo, T., Colognato, H., Zhang, X., et al. (1997). Mild congenital muscular dystrophy in two patients with an internally deleted laminin alpha2-chain. Hum. Mol. Genet. 6, 747–752.

Berthold, C.-H., and Rydmark, M. (1983). Electron microscopic serial section analysis of nodes of Ranvier in lumbosacral spinal roots of the cat: ultrastructural organization of nodal compartments in fibres of different sizes. J. Neurocytol. 12, 475–505.

Bhat, M.A., Rios, J.C., Lu, Y., Garcia-Fresco, G.P., Ching, W., St Martin, M., Li, J., Einheber, S., Chesler, M., Rosenbluth, J., et al. (2001). Axon-glia interactions and the domain organization of myelinated axons require neurexin IV/Caspr/Paranodin. Neuron 30, 369–383.

Boerkoel, C.F., Takashima, H., Stankiewicz, P., Garcia, C.A., Leber, S.M., Rhee-Morris, L., and Lupski, J.R. (2001). Periaxin mutations cause recessive Dejerine-Sottas neuropathy. Am. J. Hum. Genet. 68, 325–333.

Boyle, M.E., Berglund, E.O., Murai, K.K., Weber, L., Peles, E., and Ranscht, B. (2001). Contactin orchestrates assembly of the septate-like junctions at the paranode in myelinated peripheral nerve. Neuron 30, 385–397.

Bozic, D., Engel, J., and Brancaccio, A. (1998). Sequence analysis suggests the presence of an IG-like domain in the N-terminal region of alpha-dystroglycan which was crystallized after mutation of a protease susceptible site (Arg168→His). Matrix Biol. 17, 495–500.

Bradley, W.G., and Jenkison, M. (1973). Abnormalities of peripheral nerves in murine muscular dystrophy. J. Neurol. Sci. 18, 227–247.

Bradley, W.G., and Jenkison, M. (1975). Neural abnormalities in the dystrophic mouse. J. Neurol. Sci. 25, 249–255.

Bradley, W.G., Jaros, E., and Jenkison, M. (1977). The nodes of Ranvier in the nerves of mice with muscular dystrophy. J. Neuropathol. Exp. Neurol. 36, 797–806.

Bunge, M.B. (1993). Schwann cell regulation of extracellular matrix biosynthesis and assembly. In Peripheral Neuropathy, P.J. Dyck, P.K. Thomas, J. Griffin, P.A. Low, and J. Poduslo, eds. (Philadelphia: F. Saunders), pp. 299–316.

Byers, T., Lidov, H.G., and Kunkel, L.M. (1993). An alternative dystrophin transcript specific to peripheral nerve. Nat. Genet. 4, 77–81.

Chance, P.F. (1999). Overview of hereditary neuropathy with liability to pressure palsies. Ann. N Y Acad. Sci. 883, 14–21.

Ching, W., Zanazzi, G., Levinson, S.R., and Salzer, J.L. (1999). Clustering of neuronal sodium channels requires contact with myelinating Schwann cells. J. Neurocytol. 28, 295–301.

Cohn, R.D., and Campbell, K.P. (2000). Molecular basis of muscular dystrophies. Muscle Nerve 23, 1456–1471.

Cohn, R.D., Henry, M.D., Michele, D.E., Barresi, R., Saito, F., Moore, S.A., Flanagan, J.D., Skwarchuk, M.W., Robbins, M.E., Mendell, J.R., et al. (2002). Disruption of DAG1 in differentiated skeletal muscle reveals a role for dystroglycan in muscle regeneration. Cell 110, 639–648.

Duclos, F., Straub, V., Moore, S.A., Venzke, D.P., Hrstka, R.F., Crosbie, R.H., Durbeej, M., Lebakken, C.S., Ettinger, A.J., van der Meulen, J., et al. (1998). Progressive muscular dystrophy in alpha-sarcoglycan-deficient mice. J. Cell Biol. 142, 1461–1471.

Dupree, J.L., Girault, J.A., and Popko, B. (1999). Axo-glial interactions regulate the localization of axonal paranodal proteins. J. Cell Biol. 147, 1145–1152.

Durbeej, M., Cohn, R.D., Hrstka, R.F., Moore, S.A., Allamand, V., Davidson, B.L., Williamson, R.A., and Campbell, K.P. (2000). Disruption of the beta-sarcoglycan gene reveals pathogenetic complexity of limb-girdle muscular dystrophy type 2E. Mol. Cell 5, 141–151.

Ervasti, J.M., and Campbell, K.P. (1993). A role for the dystrophin-glycoprotein complex as a transmembrane linker between laminin and actin. J. Cell Biol. 122, 809–823.

Fannon, A.M., Sherman, D.L., Ilyina-Gragerova, G., Brophy, P.J., Friedrich, V.L., Jr., and Colman, D.R. (1995). Novel E-cadherin-mediated adhesion in peripheral nerve: Schwann cell architecture is stabilized by autotypic adherens junctions. J. Cell Biol. 129, 189–202.

Feltri, M.L., D'Antonio, M., Previtali, S., Fasolini, M., Messing, A., and Wrabetz, L. (1999). P0-Cre transgenic mice for inactivation of adhesion molecules in Schwann cells. Ann. N Y Acad. Sci. 883, 116–123.

Feltri, M.L., Porta, D.G., Previtali, S., Nodari, A., Migliavacca, B., Cassetti, A., LittleWood-Evans, A., Reichardt, L., Messing, A. Quattrini, A., Mueller, U., and Wrabetz, L. (2002). Conditional disruption of β1 integrin in Schwann cells impedes interaction with axons. J. Cell Biol. 156, 199–209.

Frei, R., Dowling, J., Carenini, S., Fuchs, E., and Martini, R. (1999). Myelin formation by Schwann cells in the absence of beta4 integrin. Glia 27, 269–274.

Gillespie, C.S., Sherman, D.L., Fleetwood-Walker, S.M., Cottrell, D.F., Tait, S., Garry, E.M., Wallace, V.C., Ure, J., Griffiths, I.R., Smith, A., and Brophy, P.J. (2000). Peripheral demyelination and neuropathic pain behavior in periaxin-deficient mice. Neuron 26, 523–531.

Gu, H., Marth, J.D., Orban, P.C., Mossmann, H., and Rajewsky, K. (1994). Deletion of a DNA polymerase beta gene segment in T cells using cell type-specific gene targeting. Science 265, 103–106.

Guilbot, A., Williams, A., Ravise, N., Verny, C., Brice, A., Sherman, D.L., Brophy, P.J., LeGuern, E., Delague, V., Bareil, C., et al. (2001). A mutation in periaxin is responsible for CMT4F, an autosomal recessive form of Charcot-Marie-Tooth disease. Hum. Mol. Genet. 10, 415–421.

Henry, M.D., Satz, J.S., Brakebusch, C., Costell, M., Gustafsson, E., Fassler, R., and Campbell, K.P. (2001). Distinct roles for dystroglycan, beta1 integrin and perlecan in cell surface laminin organization. J. Cell Sci. 114, 1137–1144.

Ibraghimov-Beskrovnaya, O., Ervasti, J.M., Leveille, C.J., Slaughter, C.A., Sernett, S.W., and Campbell, K.P. (1992). Primary structure of

dystrophin-associated glycoproteins linking dystrophin to the extracellular matrix. Nature 355, 696–702.

Imamura, M., Araishi, K., Noguchi, S., and Ozawa, E. (2000). A sarcoglycan-dystroglycan complex anchors Dp116 and utrophin in the peripheral nervous system. Hum. Mol. Genet. 9, 3091–3100.

Ishibashi, T., Dupree, J.L., Ikenaka, K., Hirahara, Y., Honke, K., Peles, E., Popko, B., Suzuki, K., Nishino, H., and Baba, H. (2002). A myelin galactolipid, sulfatide, is essential for maintenance of ion channels on myelinated axon but not essential for initial cluster formation. J. Neurosci. 22, 6507–6514.

Jaros, E., and Bradley, W.G. (1979). Atypical axon-Schwann cell relationships in the common peroneal nerve of the dystrophic mouse: an ultrastructural study. Neuropathol. Appl. Neurobiol. 5, 133–147.

Jung, D., Yang, B., Meyer, J., Chamberlain, J.S., and Campbell, K.P. (1995). Identification and characterization of the dystrophin anchoring site on beta-dystroglycan. J. Biol. Chem. 270, 27305–27310.

Komiyama, A., Novicki, D.L., and Suzuki, K. (1991). Adhesion and proliferation are enhanced in vitro in Schwann cell from nerve undergoing Wallerian degeneration. J. Neurosci. Res. 29, 308–318.

Low, P.A., Tuck, R.R., Dyck, P.J., Schmelzer, J.D., and Yao, J.K. (1984). Prevention of some electrophysiologic and biochemical abnormalities with oxygen supplementation in experimental diabetic neuropathy. Proc. Natl. Acad. Sci. USA 81, 6894–6898.

Masaki, T., Matsumura, K., Saito, F., Sunada, Y., Shimizu, T., Yorifuji, H., Motoyoshi, K., and Kamakura, K. (2000). Expression of dystroglycan and laminin-2 in peripheral nerve under axonal degeneration and regeneration. Acta Neuropathol. (Berl.) 99, 289–295.

Masaki, T., Matsumura, K., Hirata, A., Yamada, H., Hase, A., Arai, K., Shimizu, T., Yorifuji, H., Motoyoshi, K., and Kamakura, K. (2002). Expression of dystroglycan and laminin-alpha2 chain in the rat peripheral nerve during development. Exp. Neurol. 174, 109–117.

Matsumura, K., Yamada, H., Shimizu, T., and Campbell, K.P. (1993). Differential expression of dystrophin, utrophin and dystrophin-associated proteins in peripheral nerve. FEBS Lett. 334, 281–285.

Matsumura, K., Yamada, H., Saito, F., Sunada, Y., and Shimizu, T. (1997). Peripheral nerve involvement in merosin-deficient congenital muscular dystrophy and dy mouse. Neuromuscul. Disord. 7, 7–12.

Melendez-Vasquez, C.V., Rios, J.C., Zanazzi, G., Lambert, S., Bretscher, A., and Salzer, J.L. (2001). Nodes of Ranvier form in association with ezrin-radixin-moesin (ERM)-positive Schwann cell processes. Proc. Natl. Acad. Sci. USA 98, 1235–1240.

Michele, D.E., Barresi, R., Kanagawa, M., Saito, F., Cohn, R.D., Satz, J.S., Dollar, J., Nishino, I., Kelley, R.I., Somer, H., et al. (2002). Post-translational disruption of dystroglycan-ligand interactions in congenital muscular dystrophies. Nature 418, 417–422.

Moore, S.A., Saito, F., Chen, J., Michele, D.E., Henry, M.D., Messing, A., Cohn, R.D., Ross-Barta, S.E., Westra, S., Williamson, R.A., et al. (2002). Deletion of brain dystroglycan recapitulates aspects of congenital muscular dystrophy. Nature 418, 422–425.

Nakagawa, M., Miyagoe-Suzuki, Y., Ikezoe, K., Miyata, Y., Nonaka, I., Harii, K., and Takeda, S. (2001). Schwann cell myelination occurred without basal lamina formation in laminin α2 chain-null mutant (dy³ᴷ/dy³ᴷ) mice. Glia 35, 101–110.

Ohlendieck, K., and Campbell, K.P. (1991). Dystrophin-associated proteins are greatly reduced in skeletal muscle from mdx mice. J. Cell Biol. 115, 1685–1694.

Okada, E., Mizuhira, V., and Nakamura, H. (1977). Abnormally combined myelinated and unmyelinated nerves in dystrophic mice. J. Neurol. Sci. 33, 243–249.

Peles, E., and Salzer, J.L. (2000). Molecular domains of myelinated axons. Curr. Opin. Neurobiol. 10, 558–565.

Previtali, S.C., Feltri, M.L., Archelos, J.J., Quattrini, A., Wrabetz, L., and Hartung, H. (2001). Role of integrins in the peripheral nervous system. Prog. Neurobiol. 64, 35–49.

Rambukkana, A., Yamada, H., Zanazzi, G., Mathus, T., Salzer, J.L., Yurchenco, P.D., Campbell, K.P., and Fischetti, V.A. (1998). Role of

alpha-dystroglycan as a Schwann cell receptor for Mycobacterium leprae. Science 282, 2076–2079.

Rambukkana, A., Zanazzi, G., Tapino, N., and Salzer, J.L. (2002). Contact-dependent demyelination by Mycobacterium leprae in the absence of immune cells. Science 296, 927–931.

Rasband, M.N., and Trimmer, J.S. (2001). Developmental clustering of ion channels at and near the node of Ranvier. Dev. Biol. 236, 5–16.

Ratcliffe, C.F., Westenbroek, R.E., Curtis, R., and Catterall, W.A. (2001). Sodium channel beta1 and beta3 subunits associate with neurofascin through their extracellular immunoglobulin-like domain. J. Cell Biol. 154, 427–434.

Saito, F., Masaki, T., Kamakura, K., Anderson, L.V., Fujita, S., Fukuta-Ohi, H., Sunada, Y., Shimizu, T., and Matsumura, K. (1999). Characterization of the transmembrane molecular architecture of the dystroglycan complex in Schwann cells. J. Biol. Chem. 274, 8240–8246.

Scherer, S.S., and Arroyo, E.J. (2002). Recent progress on the molecular organization of myelinated axons. J. Peripher. Nerv. Syst. 7, 1–12.

Scherer, S.S., Xu, T., Crino, P., Arroyo, E.J., and Gutmann, D.H. (2001). Ezrin, radixin, and moesin are components of Schwann cell microvilli. J. Neurosci. Res. 65, 150–164.

Sherman, D.L., Fabrizi, C., Gillespie, C.S., and Brophy, P.J. (2001). Specific disruption of a schwann cell dystrophin-related protein complex in a demyelinating neuropathy. Neuron 30, 677–687.

Shetty, V. (1995). Polyaxonal myelination in a human leprous nerve. Int. J. Lepr. Other Mycobact. Dis. 63, 104–105.

Tait, S., Gunn-Moore, F., Collinson, J.M., Huang, J., Lubetzki, C., Pedraza, L., Sherman, D.L., Colman, D.R., and Brophy, P.J. (2000). An oligodendrocyte cell adhesion molecule at the site of assembly of the paranodal axo-glial junction. J. Cell Biol. 150, 657–666.

Thouvarecq, R., Protais, P., Jouen, F., and Caston, J. (2001). Influence of cholinergic system on motor learning during aging in mice. Behav. Brain Res. 118, 209–218.

Tsiper, M.V., and Yurchenco, P.D. (2002). Laminin assembles into separate basement membrane and fibrillar matrices in Schwann Cells. J. Cell Sci. 115, 1005–1015.

Wacnik, P.W., Eikmeier, L.J., Ruggles, T.R., Ramnaraine, M.L., Walcheck, B.K., Beitz, A.J., and Wilcox, G.L. (2001). Functional interactions between tumor and peripheral nerve: morphology, algogen identification, and behavioral characterization of a new murine model of cancer pain. J. Neurosci. 21, 9355–9366.

Williamson, R.A., Henry, M.D., Daniels, K.J., Hrstka, R.F., Lee, J.C., Sunada, Y., Ibraghimov-Beskrovnaya, O., and Campbell, K.P. (1997). Dystroglycan is essential for early embryonic development: disruption of Reichert's membrane in Dag1-null mice. Hum. Mol. Genet. 6, 831–841.

Yamada, H., Shimizu, T., Tanaka, T., Campbell, K.P., and Matsumura, K. (1994). Dystroglycan is a binding protein of laminin and merosin in peripheral nerve. FEBS Lett. 352, 49–53.

Yamada, H., Denzer, A.J., Hori, H., Tanaka, T., Anderson, L.V., Fujita, S., Fukuta-Ohi, H., Shimizu, T., Ruegg, M.A., and Matsumura, K. (1996). Dystroglycan is a dual receptor for agrin and laminin-2 in Schwann cell membrane. J. Biol. Chem. 271, 23418–23423.

Yeomans, D.C., and Proudfit, H.K. (1996). Nociceptive responses to high and low rates of noxious cutaneous heating are mediated by different nociceptors in the rat: electrophysiological evidence. Pain 68, 141–150.